Acta Crystallographica Section B
Structural Science, Crystal Engineering and Materials
ISSN 2052-5206

Charge distribution as a tool to investigate structural details. III. Extension to description in terms of anion-centred polyhedra

Jean-Guillaume Eon and Massimo Nespolo

Acta Cryst. (2015). B**71**, 34–47

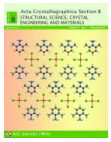

Acta Crystallographica Section B
Structural Science, Crystal Engineering and Materials
ISSN 2052-5206

Charge distribution as a tool to investigate structural details. III. Extension to description in terms of anion-centred polyhedra

Jean-Guillaume Eon[a]* and Massimo Nespolo[b]

[a]Instituto de Química, Universidade Federal do Rio de Janeiro, Avenida Athos da Silveira Ramos, 149 Bloco A, Cidade Universitária, Rio de Janeiro 21941-909, Brazil, and [b]Université de Lorraine, Faculté des Sciences et Technologies, Institut Jean Barriol, FR 2843, CRM2 UMR – CNRS 7036, BP 70239, Boulevard des Aiguillettes, F54506 Vandoeuvre-lès-Nancy CEDEX, France

Correspondence e-mail: jgeon@iq.ufrj.br

Received 16 August 2014
Accepted 9 December 2014

The charge distribution (CHARDI) method is a self-consistent generalization of Pauling's concept of bond strength which does not make use of empirical parameters but exploits the experimental geometry of the coordination polyhedra building a crystal structure. In the two previous articles of this series [Nespolo *et al.* (1999). *Acta Cryst.* B**55**, 902–916; Nespolo *et al.* (2001). *Acta Cryst.* B**57**, 652–664], we have presented the features and advantages of this approach and its extension to distorted and heterovalent polyhedra and to hydrogen bonds. In this third article we generalize CHARDI to structures based on anion-centred polyhedra, which have drawn attention in recent years, and we show that computations based on both descriptions can be useful to obtain a deeper insight into the structural details, in particular for mixed-valence compounds where CHARDI is able to give precise indications on the statistical distribution of atoms with different oxidation number. A graph-theoretical description of the structures rationalizes and gives further support to the conclusions obtained *via* the CHARDI approach.

1. Introduction

Since Pauling's (1929) pioneering work introducing the concept of bond strength, a significant number of studies have been devoted to the effort of developing simple yet powerful tools to analyse the connectivity of crystal structures. This connectivity – how and how far an atom is bonded to its neighbours in a certain structure under given experimental conditions – is the simplest feature we can extract from the atomic coordinates and the result of both the thermodynamic and kinetic conditions in which the structure was formed. In particular, a structure with low kinetic constraints, close to its equilibrium, will show a low degree of over- or under-bonding on each of its atoms. A quantification of this over-/under-bonding is thus a measure of the state of the structure and an indication of its susceptibility to evolve and release the accumulated constraints (diffusion, charge transfers, phase transitions, domain formation *etc.*).

Very fine details can nowadays be obtained on the atomic and electronic structure of molecular compounds, provided that excellent experimental data at high resolution are available; on the other hand, some characteristic features of non-molecular structures which do not commonly occur in molecular compounds, like the presence of isomorphic substitutions, are not necessarily taken into account in the algorithms and software packages devoted to the analysis of the electron densities (Zarychta *et al.*, 2007). *Ab initio* quantum-chemical analysis of crystal structures are becoming more and more

accessible, but their target is more on complex electronic interactions – besides the fact that a quantum-chemical analysis of relatively simple problems like the connectivity of crystal structures would correspond to cracking a nut with a sledgehammer.

An ideal tool for the study of connectivity of crystal structures is graph theory, of which some examples of applications are given in this article. Today, powerful tools like *TOPOS* (Blatov *et al.*, 2014) are available, but for this analysis the 'strength' of each bond and the results of the distribution of this 'strength' about each atom need a quantitative measure. Pauling's bond strength was introduced for uniform coordination polyhedra[1] as the ratio of the 'charge' (formal oxidation number) to the coordination number of the electropositive atom. For general polyhedra, the concept of coordination number is less well defined (Hoppe, 1970) and an apparently simple concept like the ionic radius needs corrections for coordination number and valence (Zachariasen, 1931; see also the discussion in Beck, 2014); furthermore, a dependence of the bond strength from the bond length had to be introduced. This had actually been recognized since before Pauling's landmark paper (see Zachariasen, 1978*a*) and was obtained through the use of empirical curves (commonly called '*R*–*s* curves'), whose parameters are obtained by fitting on a large set of structures, in what is known as the bond valence (BV) method (Brown, 1978). A general expression of the *R*–*s* curve can be written in the form $s = s_0(R/R_0)^{-N}$, where R is bond distance and where up to three kinds of empirical parameters are used: R_0, the *normalizing parameter*, close to the mean bond distance; N, the *contraction parameter*, responsible for the decreasing weight of each bond with the distance; and s_0, a *scaling parameter* (Nespolo *et al.*, 1999). The coordination number is obtained *a posteriori* by counting the number of neighbours for which bond valence is significant.

The BV approach presents some limitations:

(i) the empirical parameters are characteristic of the pair of atoms involved in a chemical bond;

(ii) the refined parameters depend on the experimental conditions on which the representative set of structures has been obtained, and the extrapolation to different conditions can be problematic;

(iii) the empirical parameters are far from established for all and may depend even on the type of polyhedra (Mills *et al.*, 2009);

(iv) a tendency to try to extract information hardly present in such a simple analysis, in particular electronic details, from the *R*–*s* curves is often seen in the literature.

A fundamentally different approach was introduced by Hoppe (1979) and Hoppe *et al.* (1989) with the concepts of effective coordination number (ECoN) and charge distribution (CHARDI), where the *normalizing*, *contraction* and *scaling* parameters are no longer the result of a fit but directly related to the geometry of each coordination polyhedron and the formal charge (oxidation number) of the atoms building the crystal structure. In the two previous articles of this series (Nespolo *et al.*, 1999; 2001) we have presented this approach and its generalization to distorted polyhedra, hydrogen bonds and heteroligand polyhedra, as well as a comparison to other methods used to analyse the connectivity of crystal structures. In this third part we present a further extension, to anion-centred polyhedra.

2. ECoN and CHARDI for generalized polyhedra

In the CHARDI approach, atoms are considered in the classical Madelung's description as point charges where the formal 'charge' corresponds to the oxidation number. This description does not imply, however, the presence of ionic bonds, but simply the existence of bonds between electropositive and electronegative atoms, which will be hereafter termed 'cations' and 'anions' for the sake of briefness due to the positive and negative formal charge attributed to them.

ECoN can be defined for any type of coordination, including incomplete polyhedra and general valence compounds (*i.e.* compounds in which either the cations do not transfer all their valence electrons or the anions do not need as many electrons from the cations to complete their octet shells; Parthé, 1996); the CHARDI analysis, instead, in general is not applicable to polyions (see, however, the examples in Nespolo *et al.*, 2001), as well as compounds with delocalized electrons (metallic bond).

The CHARDI approach has so far been presented by assuming the cations at the centre of the coordination polyhedra. This description is the classical one and is suitable for most compounds: the fact that anions have, in general, larger size leads them to occupy the larger part of the crystal volume, while cations fit the holes formed by the anion distribution. However, in relatively recent years a number of examples have been reported of compounds having anion-centred groups which are condensed in a more complicated manner than the cation-centred groups. Some enlightening examples are considered in the next section; see a comprehensive review in Krivovichev (2009) and Krivovichev *et al.* (2013). These examples have prompted us to implement an extension of CHARDI analysis where the role of cations and anions can be exchanged. The CHARDI equations are thus presented here in a revised form, where atoms in a crystal structure are classified as 'polyhedron-centring atoms' (**PC atoms**) and 'vertex (corner) atoms' (**V atoms**). The assignment of cations and anions to each of the two categories can be interchangeable.

PC atoms and V atoms are indicated as PC(ij) and V(rs), respectively, where i and r identify the atomic site, whereas j and s refer to the crystallographic type. The formal charges (which become the weighted average in isomorphic substitutions) are indicated as $q(ij)$ and $q(rs)$, which depend on j or s through the site occupation factor (s.o.f.): for s.o.f. = 1, all the PC atoms with the same i, as well as all the V atoms with the same r, have the same q. Similarly, the multiplicity of the Wyckoff position is indicated as $h(ij)$ and $h(rs)$. The Lth bond length between PC(ij) and V(rs) is indicated as $d(ij \rightarrow rs)_L$.

[1] Regular, quasi-regular and semi-regular polyhedron, *i.e.* polyhedra in which the distances from the centre to the vertices are all identical.

For computational purposes, the bond lengths are classified in increasing length with respect to i, j and r; $d(ij \rightarrow rs)_1$ being the shortest and s a sort of dummy index at this stage.

The mean PC—V distance in each polyhedron is computed through a weighted average[2]

$$
\begin{aligned}
{}^{n}d(ij \rightarrow r) &= \frac{\sum_s \sum_L d(ij \rightarrow rs)_L \cdot {}^{n-1}w(ij \rightarrow rs)_L}{\sum_s \sum_L {}^{n-1}w(ij \rightarrow rs)_L} \\
{}^{n-1}w(ij \rightarrow rs)_L &= \exp\left\{1 - \left[\frac{d(ij \rightarrow rs)_L}{{}^{n-1}d(ij \rightarrow r)}\right]^6\right\} \\
{}^{0}d(ij \rightarrow r) &= d(ij \rightarrow rs)_1,
\end{aligned} \tag{1}
$$

where n is an iteration index and the weight ${}^{n-1}w(ij \rightarrow rs)$ takes the form of an exponential responsible for the asymptotic decrease of the contribution of each bond with the increasing of its length. The shortest PC—V distance in each polyhedron is used as a *normalizing parameter* at the zeroth stage of the iteration, to be replaced by the weighted average until convergence is reached (see *Appendix A* for proof that the iterative process is convergent).

The 'strength' of the $d(ij \rightarrow rs)_L$ bond is measured by the *bond weight* $\mathrm{BW}(ij \rightarrow rs)_L$, which is simply an expression of the weight $w(ij \rightarrow rs)$ once convergence is reached[3]

$$
\mathrm{BW}(ij \rightarrow rs)_L = w(ij \rightarrow rs)_L = \exp\left\{1 - \left[\frac{d(ij \rightarrow rs)_L}{{}^{n}d(ij \rightarrow r)}\right]^6\right\}. \tag{2}
$$

Finally, the sum over the bond weights gives the effective coordination number (ECoN), defined both in terms of PC(ij) and V(r), $\mathrm{ECoN}(ij \rightarrow r)$, and of PC($ij$) only, $\mathrm{ECoN}(ij)$

$$
\begin{aligned}
\mathrm{ECoN}(ij \rightarrow r) &= \sum_s \sum_L \mathrm{BW}(ij \rightarrow rs)_L \\
\mathrm{ECoN}(ij) &= \sum_r \mathrm{ECoN}(ij \rightarrow r).
\end{aligned} \tag{3}
$$

ECoN, as a generalization of the classical coordination number, is a *real* number that has to become equal to the integer coordination number for uniform polyhedra. This is the condition imposed to obtain the *contraction parameter* 6 in the definition of the weight $w(ij \rightarrow rs)$. It was in fact obtained by finding the highest value giving an ECoN equal to the number of first neighbours in the structure of simple metals, where a clear separation between a first and a second coordination sphere exists (Hoppe, 1979). For the very special case of hydrogen bonds, where the ratio of two short distances (donor-H and H-acceptor) with a high relative gap made the weight $w(ij \rightarrow rs)$ for the second bond negligible, a revised contraction parameter of 1.6 has been introduced (Nespolo *et al.*, 2001).

CHARDI distributes $\mathrm{ECoN}(ij \rightarrow r)$ among all the bonds around each PC(ij), obtaining in this way the contribution by each V(rs) to $\mathrm{ECoN}(ij \rightarrow r)$ itself

$$
\Delta\mathrm{ECoN}(ij \rightarrow rs) = \frac{\sum_L \mathrm{BW}(ij \rightarrow rs)_L}{\mathrm{ECoN}(ij \rightarrow r)}. \tag{4}
$$

As equation (4) clearly shows, this is a geometrical analysis of the connectivity of the crystal structure. In a correctly refined and well balanced structure, the distribution of ECoN among the PC—V bonds should sum up to some expected value for both PC(ij) and V(rs). As the expected value, the formal charge is used: ΔECoN is multiplied by the *scaling parameter* $q(ij)$. A scale factor $F(ij \rightarrow r)$ is also introduced for heteroligand polyhedra (Nespolo *et al.*, 2001)

$$
\Delta q(ij \rightarrow rs) = \Delta\mathrm{ECoN}(ij \rightarrow rs) q(ij) F(ij \rightarrow r). \tag{5}
$$

When summing on the PC atoms about a V atom, one should obtain the expected 'charge' of the V atom itself

$$
Q(rs) = -\sum_i \sum_j \Delta q(ij \rightarrow rs) \frac{h(ij)}{h(rs)}. \tag{6}
$$

The ratio of the multiplicities of the respective Wyckoff positions, $h(ij)/h(rs)$, is introduced to avoid counting multiple contributions when a bond relates atoms on Wyckoff positions with different multiplicities.

A similar distribution is repeated the other way round and summed up on the V atoms about a PC atom. This time, however, instead of using $q(rs)$ as the scaling parameter, in a perfectly symmetrical way, the ratio $q(rs)/Q(rs)$ for the V(rs) bonded to PC(ij) is used

$$
\begin{aligned}
Q(ij) &= \left[\sum_r \sum_s \Delta\mathrm{ECoN}(ij \rightarrow rs) \frac{q(rs)}{Q(rs)} F(ij \rightarrow r)\right] \\
q(ij) &= \sum_r \sum_s \Delta q(ij \rightarrow rs) \frac{q(rs)}{Q(rs)}.
\end{aligned} \tag{7}
$$

If $q(rs)/Q(rs) = 1$ for each r and s, then the bracket in equation (7) goes to 1 (it becomes the sum of the fractions of ECoN about each PC atom) and thus $Q(ij) = q(ij)$. This shows that in a structure correctly solved and perfectly valence-balanced, the distribution of ECoN scaled by the formal charges gives back these charges. On the other hand, when a structure has developed some structural tensions, its V atoms may not be perfectly balanced but the distribution of this unbalance, measured by the ratio $q(rs)/Q(rs)$, should give back the expected formal charges on the PC atoms, otherwise the whole set of coordination polyhedra would be unbalanced and the structure would be unstable. In other words, CHARDI possesses an internal criterion to evaluate the quality of its analysis: the ratio $q(ij)/Q(ij)$ for the PC atoms. When this ratio is reasonably close to 1, then the analysis of the connectivity can be approached by the study of $Q(rs)$, which diverge from $q(rs)$ proportionally to the structural strains inside the structure. One speaks of the *over–under-bonding (OUB) effect* (Nespolo *et al.*, 1999, 2001). Quite obviously, in the trivial case

[2] With respect to the previous articles, to simplify the equations we have dropped the multiplicity of the bond distances: when multiple bonds correspond to the same distance for symmetry reasons, they are simply counted separately in the summation.

[3] In the previous article (Nespolo *et al.*, 2001), when the iterative calculation of ECoN was introduced we used the notation ^{n}ECoN to differentiate the values of ECoN obtained with and without iteration and emphasize the better results given by this procedure in the presence of significant deformation of the coordination polyhedron. The non-iterative calculation being no longer used, here we drop the exponent ^{n} in all quantities but ${}^{n}d(ij \rightarrow r)$ to simplify the notation.

of structures containing only one type of V atom there is nothing to distribute, $Q(rs)$ is identical to $q(rs)$ and the CHARDI analysis simply does not apply.

As an overall measure of the agreement between q and Q for the whole sets of PC atoms and of V atoms, the *mean absolute percentage deviation* (MAPD) is used

$$\mathrm{MAPD} = \frac{100}{N}\sum_{i=1}^{N}\left|\frac{q_i - Q_i}{q_i}\right|. \qquad (8)$$

MAPD is preferred to the data dispersion used in previous versions of the algorithm, defined as a sort of generalization of standard deviation, because the latter tends to overestimate the deviation, especially in the case of a small number of atoms. Although it is not possible to indicate a precise threshold above which the result should be considered unacceptable, it is quite obvious that the expected MAPD value on the PC atoms is lower than that expected on the V atoms, because the former is a signature of the correctness of the structure and of the applicability of the model, whereas the latter measures the OUB effect. A statistical analysis of a large number of samples would be necessary to give precise intervals, but as a rule of thumb a value above 10% for the PC atoms seriously questions the interpretation of the analysis, or possibly the correctness of the refinement. For V atoms, a value below 5% indicates the low OUB effect, which then increases proportionally to MAPD. A value about 20% seems hardly meaningful, because it would correspond to a strong OUB effect which would probably make the structure unstable: it could however be realised in metastable structures quenched outside their stability region.

PC atoms and V atoms were previously identified with cations and anions, respectively. We are going to show through a series of examples discussed in detail that:

(i) some structures which would be unacceptable when described as cation-centred actually find their rationale if a description as anion-centred is adopted; and

(ii) the parallel analysis of the results in both descriptions sometimes reveals details that would escape when only one description is adopted.

To make this analysis as clear as possible and to avoid any possible confounding factor coming from the presence of the hetero-ligand polyhedra in one description but not in the other, we have chosen binary compounds for the following discussion.

3. Why anion-centred polyhedra?

Living in an oxygen-rich environment we have probably overestimated the structural role of cation-centred polyhedra that are so neatly defined in a geometric sense in higher metal oxides. However, we should expect that electronegative atoms diluted in a metallic solvent such as occurs in lower metal oxides give way to anion-centred polyhedra. The case of cuprite is well known: It is hardly possible to use the linear coordination of Cu as a structural descriptor and one is clearly led to consider Cu_2O as consisting of corner-sharing $[OCu_4]$ tetrahedra. Similarly the elusive sodium nitride Na_3N with the *anti*-ReO_3-type structure consists of corner-sharing $[NNa_6]$ octahedra (Fischer & Jansen, 2002). Sub-stoichiometric oxides are no less interesting, although not so many compounds are described in structural databases and the CHARDI analysis does not necessarily apply to all of them, in particular when the coordination environment of an atom includes atoms of the same family (*e.g.* in the presence of metallic bonds).

In such oxides as Ti_3O, $V_{14}O_6$ or Zr_3O only octahedral coordination of O is clearly defined. In lower Cs oxides, face-sharing oxo-centred octahedra $[OCs_6]$ are present as clusters of three octahedra with a common edge in Cs_4O and $Cs_{11}O_3$ or as infinite columns in Cs_3O, which is anti-isopointal with β-$TiCl_3$. Even the structural chemistry of alkaline oxides is worth reviewing in this perspective. Almost all these M_2O oxides adopt the antifluorite structure with the exception of Cs_2O, which is anti-isotypic with $CdCl_2$. Owing to the 2:1 stoichiometry, the antifluorite structure is composed of $[MO_n]$ cation-centred polyhedra and $[OM_{2n}]$ oxo-centred polyhedra. In the case of Rb_2O the $[RbO_4]$ tetrahedron is probably under high stress due to the similar size of both ions, and the structure is probably stabilized by the cubic coordination of O. However, both tetrahedral coordination of Cs and cubic coordination of O seem to be untenable in Cs_2O, the structural motifs of which are octahedral $[OCs_6]$ and trigonal pyramidal $[CsO_3]$.

We notice that most compounds described as anion-centred in Krivovichev (2009) and Krivovichev *et al.* (2013) have been considered to possess an additional oxygen atom, which for this atom corresponds to low concentration. Thus, in general, stoichiometry should be considered as one of the relevant factors, along with ionic size and other chemical properties, in order to estimate the relative structural significance of cation- and anion-centred polyhedra, but both should definitely be taken into account as complementary aspects of the topology of crystal structures.

There is, however, a further reason to sometimes adopt an anion-centred description, even if the topology of the crystal structure does not call for it. As shown by equation (6), the charge of a V atom is computed as a function of the charges of the PC atoms bonded to it. Let M_mA_a be the maximally simplified formula for a compound under consideration, containing m 'cations' (electropositive atoms) M and a 'anions' (electronegative atoms) A. Let one or more sites be statistically occupied by more than one M (A, respectively) with different formal charge (the chemical species can be equal or different). By treating M (A) as a V atom, CHARDI computation suggests a formal charge for the site, which is indicative of the statistical occupancy of this site. In the case of atoms of the same chemical species, this information can be difficult to obtain from the experimental data, while CHARDI can instead provide a decisive indication. The same is true when M (A) atoms with variable valence coexist in the same structure: the difference between the pair $M_i^{p+}M_j^{q+}$ and $M_i^{(p-n)+}M_j^{(q+n)+}$ or between $A_i^{p-}A_j^{q-}$ and $A_i^{(p-n)-}A_j^{(q+n)-}$ may be hard to establish, while CHARDI gives a clear indication if M (A) is treated as a V atom. On the other hand,

because the charges of the PC atoms are computed as a function of the ratio q/Q of the computed and input charges of V atoms [equation (7)], the result does not provide similar information. In other words, by describing a structure containing isomorphous substitutions on M (A) first of all as A-centred (M-centred), important indications about the formal charge of the M (A) site can be obtained which can then be exploited to provide the opposite description, centred on M (A). Because isomorphous substitutions are much more common among cations, this procedure will be used more often to estimate the charges of a cation site on the basis of an anion-centred description; the opposite case is certainly less common. As an illustrative example, in the following we present this type of procedure applied to the case of Magnéli phases.

4. Bond graphs and digraphs

Data concerning the structure of chemical compounds are commonly summarized in the form of a *graph*, where atoms are symbolized by a *vertex* (or a point) and a bond between two atoms is symbolized by an *edge* (or a line) joining the corresponding vertices; this graph is called the *bond graph* of the structure. It is trivial, for instance, to write the structure of the molecule of water as H—O—H: this is a graph with three vertices (H, O, H) and two edges noted as a link (—) between pairs of atoms. It must be stressed that no hypothesis is made here about the nature of the bond. In particular, the link (—) does not refer to a Lewis electron pair, it only expresses the fact that these atoms are bonded. The general question is: How can we know which atoms are bonded in a given structure, and how are we to represent the bond graph of an infinite solid? As mentioned above, atomic (ionic) radii cannot be relied upon to find pairs of bonded atoms in low-symmetry structures. The theory of atoms in molecules (AIM; Bader, 1994) is the only quantum-mechanical theory applicable to open systems. AIM characterizes a bond as a critical point with the right signature in the electronic density of molecules or solids. This density may be obtained on theoretical grounds, using *ab-initio* quantum chemical calculations, or on experimental grounds using density maps derived from high-resolution diffraction techniques. In the absence of such data, the CHARDI method proposes *a posteriori* computations to determine coordination polyhedra in solids based on a very simple hypothesis, and using only geometrical information. However, dichotomy between cations and anions yields two interpretations of the structure which may be in agreement but sometimes seems to be in contradiction, so that the bond graph may be ill-defined. To remedy real or apparent discrepancies, we introduce the concept of the bond digraph, which will be better explained using an example (see also the Glossary in *Appendix C*). Although the next section deals with the topological properties of the structure, charge distribution results will be discussed at the same time to avoid any discontinuity in the analysis of structural details.

Table 1
CHARDI coordination polyhedra in B_2O_3-I ($P3_1$); distances in Å.

	O1	O2	O3
B1	1.404	1.366	1.336
B2	1.338	1.403	1.386

Table 2
CHARDI computation results for B_2O_3-I ($P3_1$).

	B1	B2	O1	O2	O3	MAPD
Cation-centring	3.00	3.00	−2.01	−1.89	−2.10	(0, 3.5%)
Anion-centring	3.03	2.97	−2.00	−2.00	−2.00	(0.1, 1.0%)

4.1. B_2O_3: a case study

We apply CHARDI to analyze some structural details concerning the crystal structure of diboron trioxide; this will lead to defining the corresponding bond digraph. We look first at the well behaved low-pressure trigonal B_2O_3-I phase whose structure was published by Gurr *et al.* (1970). The asymmetric unit (space-group type $P3_1$) contains two B and three O atoms. Tables 1 and 2 display some computation results obtained by CHARDI, running with cation-centred and anion-centred polyhedra. Bond lengths display a rather small dispersion in this structure and this makes it possible to cast the five kinds of coordination polyhedra (BO_n and OB_m) determined by CHARDI as a single array, which is displayed in Table 1. Running the cation-centring routine of CHARDI, one finds that every B atom is coordinated to three O atoms, one of each type, which is in agreement with classical views about this structure. Conversely, running the anion-centring routine one sees that every O atom is coordinated to two B atoms, one of each type. Rows in Table 1 give bond lengths in cation-centred coordination polyhedra and columns give bond lengths in anion-centred polyhedra. These data allow the construction of the bond graph shown in Fig. 1. Explicitly, the bond graph has five vertices: two for B atoms (Bi, i = 1, 2) and three for O atoms (Oj, j = 1, 2, 3), and six edges: one for each bonded pair (Bi,Oj), i = 1, 2 and j = 1, 2, 3.

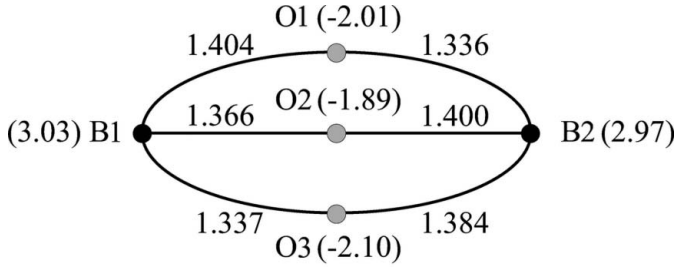

Figure 1
Graph of the asymmetric unit of B_2O_3-I including bond lengths (Å) and charge distribution (CHARDI) computation results within brackets. B atoms are shown in black and O atoms in grey.

Table 2 gives the computed charge distribution on each kind of atom with cation-centred polyhedra (first row) and anion-centred polyhedra (second row). In both cases, MAPD are indicated as a couple of values where the first one refers to the PC atom on the respective row. The null MAPD obtained on PC atoms in both situations shows that both descriptions are consistent and meaningful. This result enables a joint interpretation of the charge distributions obtained from cation- and anion-centring routines, which will be advantageously performed using the bond graph. Because MAPD are null at the PC atoms, input charges (in fact formal oxidation numbers) were not reported in the figure. Thus, charges displayed at B/O atoms are those calculated by the anion-/cation-centring routine of CHARDI. This way, the bond graph in Fig. 1 combines:

(i) structural information corresponding to the asymmetric unit of the crystal structure and

(ii) charge distribution computed by CHARDI.

Interpretation of the data is based on bond lengths, which is also reported in the bond graph. In fact, CHARDI computes weighted average bond lengths for each polyhedron using exponential weights [equation (1)], but in this simple structure it is clear that B1—O distances (CHARDI average: 1.365 Å) are slightly shorter than B2—O distances (CHARDI average: 1.370 Å). Similarly, centring on the anion gives the following average distances.

$$\text{CHARDI}: \begin{cases} d(\text{O1}-\text{B}) = 1.365\ \text{Å} \\ d(\text{O2}-\text{B}) = 1.382\ \text{Å} \\ d(\text{O3}-\text{B}) = 1.358\ \text{Å} \end{cases}$$

Charge distribution naturally correlates with these average distances. Thus, the B1 atom being closer on average to its three O neighbours than the B2 atom appears to be over-bonded in this structure. The O2 atom being farther from its two B neighbours than O1 and more particularly than O3 is under-bonded, whereas the latter is over-bonded.

A refinement of the structure of the B_2O_3-I phase was more recently published by Effenberger *et al.* (2001) who concluded that this structure belongs to the higher space-group type $P3_121$. The asymmetric unit in this space-group type contains only one B atom and two O atoms. Table 3 shows the bond lengths for coordination polyhedra determined by CHARDI using both the cation-centring routine (first row) and the anion-centring routine (second and third rows). This table is clearly asymmetric: B atoms make one bond to O2 atoms, but these make two bonds to B atoms. Such asymmetry forbids the construction of a bond graph but still allows the construction of a bond digraph. By definition, the edges in a digraph are directed, or one-way. So we may represent the set of bonds between B and O2 in this structure by a digraph with two vertices, B and O2, and three directed edges between B and O2, one outgoing edge and two incoming edges at vertex B, as in Fig. 2, where the direction of each edge is indicated by an arrow. However, before we can validate such a construct and obtain a full understanding of its meaning, we need to go back to a bond graph representing the entire three-dimensional structure.

Table 3
CHARDI coordination polyhedra in B_2O_3-I ($P3_121$); distances in Å.

	B	O1	O2
B	–	(1.372, 1.376)	1.357
O1	(1.372, 1.376)	–	–
O2	(1.356, 1.357)	–	–

Fundamentally, we will not need the infinite bond graph of the whole structure but only a finite representative bond graph, the vertex set of which corresponds to the set of atoms in a primitive unit cell. In this particular case, bond graphs are called *quotient graphs*. A quotient graph represents the network of interatomic bonds for the set of atoms obtained by applying to each atom in the unit cell the full set of translations of the space group, *i.e.* the $P1$ *translationengleiche* subgroup (*t*-subgroup) of the space group G. An atom occupying a Wyckoff position of multiplicity M generates, under the action of G, a crystallographic orbit (Engel *et al.*, 1984). When the $P1$ *t*-subgroup is applied instead, this orbit is split into a set of M suborbits, which in graph theory are called *point-lattices* (Chung *et al.*, 1984). Point-lattices are taken as vertices of the quotient graph; two point-lattices are linked by an edge in the quotient graph whenever two atoms of the respective suborbits are bonded in the crystal structure. Multiple edges occur when an atom in some point-lattice is linked to more than one atom in another, or the same point-lattice.

The refinement of the structure of B_2O_3 proposed by Effenberger *et al.* (2001) only affects the symmetry and not the structural framework of the B_2O_3-I phase. The following analysis is therefore independent of the symmetry assignment. Let us start from the structure of highest symmetry. There are 3 unit formulae in the primitive cell. B and O1 atoms occupy general positions (site symmetry 1) with multiplicity 6, while O2 atoms are on special positions (site symmetry .2.) with multiplicity 3. Hence, the quotient graph contains six atoms of type B, six of type O1 and three of type O2. There are many possibilities to insert edges according to Table 3; the correct graph, shown in Fig. 3, may be recovered using the package *TOPOS* (Blatov *et al.*, 2014), for example after decreasing symmetry down to space-group type $P1$.

Clearly, the quotient graph alone does not permit to recover the three-dimensional structure. It only tells us about the

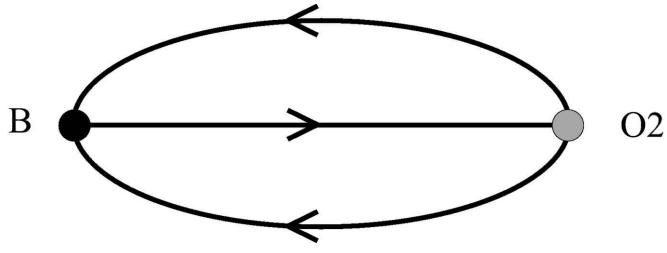

Figure 2
A digraph on the vertices B and O2.

existence of bonds between atoms belonging to the different point-lattices, but it does not specify which atoms in these point-lattices are bonded. This can be done using the labelled quotient graph, as explained in *Appendix B*. Here we are mainly concerned with the determination of the bond digraph of the asymmetric unit and this can be performed directly from the quotient graph.

Let $U = \{u_i\}$, $V = \{v_j\}$ be two vertex-orbits in the bond graph of a crystal structure S under its space group G; then every vertex in the set U is linked in S to the same number, say n, of vertices in the set V. We can thus define a multiple (n-folded) edge directed from U to V in the quotient digraph S/G. We stress that vertices in set V are generally not linked to the same number n of vertices in set U. This happens when bonded atoms occupy sites with different multiplicity, in which case the previous definition becomes inevitable. Note also that the determination of the bond digraph can be done directly on the quotient graph since there is no invariant atom by translation. For instance, every B atom in B_2O_3-I is linked to a single oxygen atom in the set O2, but every oxygen atom in the set O2 is linked to two B atoms. This shows that we cannot define the number of (conventional) edges between B and O2: there is no consistent definition of a quotient graph in this case. We must define a digraph with a single directed edge from B to O2 and two directed edges from O2 to B. In contrast, two edges link every atom in B to atoms in O1 and conversely two edges link every atom in O1 to atoms in B. Notice that directed edges can be assigned symmetry operations (Klein, 1996; see also Eon, 2012, for a comparison with symmetry-labelled quotient graphs). The symmetry-labelled quotient digraph of B_2O_3-I is shown in Fig. 4 with assignment in $P3_121$; notice the symmetry labels (*voltages*) such as $\gamma = 010.2.3_1$ (the threefold screw rotation 3_1 followed by the twofold rotation 2 and finally by the translation 010) attributed to edge B—O1 indicating that atom B[g] is linked to atom O1[$g\gamma$] (see also the Glossary in *Appendix C*).

Symmetry-labelled quotient digraphs must be carefully handled, but they bear similar properties to labelled quotient graphs. In particular, they still give a faithful representation of the local topology of the crystal structure if one considers only outgoing edges for each kind of atom. We may also define a reduced quotient digraph as follows. Observe first that three edges in Fig. 4 can be paired with another edge with the same end-vertices in such a way that one edge out of each pair has the inverse symmetry label (*voltage*) of the other edge of the pair. For example, the edge O2–B with voltage 2 can be paired with the unique edge B–O2, also with voltage 2. Paired edges correspond to the same edge with opposite orientation in the bond graph of the crystal structure. As mentioned at the beginning of this section, the fact that there are two directed O2–B edges and a single B–O2 edge means that B and O2 occupy sites with different multiplicities. In this case, we can deduce the site symmetry of O2 as follows. Let us denote by $A[g]$ the atom mapped by applying the symmetry operation g to atom A at the origin of the respective point-lattice. We read from the symmetry-labelled quotient digraph in Fig. 4 that O2 is linked to B and to B[2]. Similarly, we read that B and B[2] are linked respectively to O2[2] and O2[2.2] = O2. It follows that O2 and O2[2] are the same atom, hence that O2 has site symmetry .2.. From the viewpoint of the charge distribution method it is enough to report independent edges, as shown in Fig. 5. By definition every *UV* edge of the reduced quotient digraph carries an n-folded arrow from vertex U, indicating that n symmetry-equivalent edges in the bond graph of the crystal structure connect any atom in vertex-orbit U to n atoms in vertex-orbit V. For example, the double arrow out of vertex O2 on edge O2–B in the reduced digraph means that two directed edges go from O2 to B in the symmetry-labelled

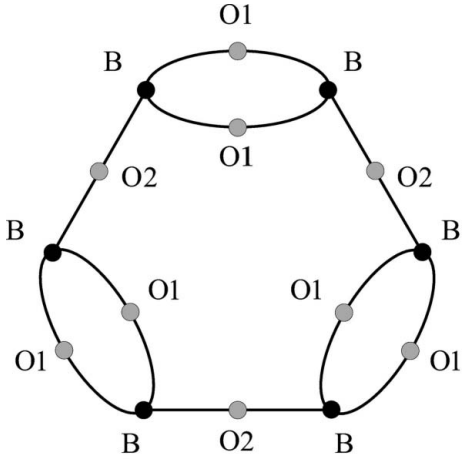

Figure 3
The quotient graph G of B_2O_3-I; B atoms are shown in black and O atoms in grey. Atom types are in accordance with the space-group type $P3_121$.

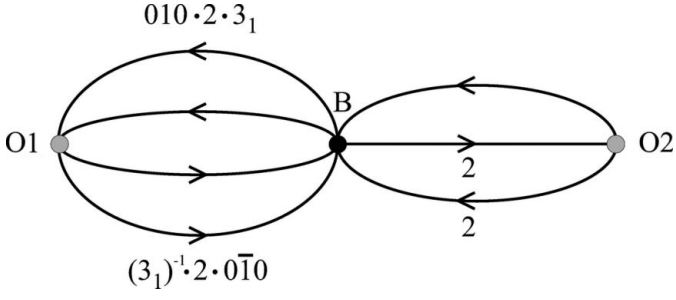

Figure 4
The symmetry-labelled quotient digraph of B_2O_3-I with respect to the space-group type $P3_121$; B atoms are shown in black and O atoms in grey.

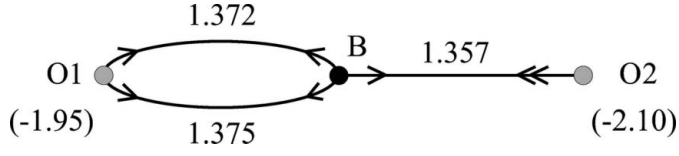

Figure 5
The reduced quotient digraph of B_2O_3-I with respect to the refined space-group type $P3_121$; B atoms are shown in black and O atoms in grey. Bond lengths (Å) are indicated above each edge and charge distribution (CHARDI) computation results for O atoms within brackets. See text for interpretation of simple and double arrows.

quotient digraph, the two corresponding edges being symmetry-equivalent in B_2O_3-I. If n_U and n_V are the number of symmetry-equivalent edges UV from vertices U and V, respectively, the ratio n_V/n_U is equal to the inverse ratio h_U/h_V of the multiplicities of corresponding atom types in the crystal structure.

Charge distribution (CHARDI) computation results for cation-centred polyhedra are indicated within brackets in Fig. 5 with a MAPD of (0, 3.3%). Anion-centred polyhedra give (0, 0) MAPD; this result is a trivial consequence of the symmetry of the reduced quotient digraph which reflects the fact that the structure contains only one type of cation and has no physical meaning. Again, interpretation of the results in the case of cation-centred polyhedra may be based on weighted average bond lengths.

$$\text{CHARDI}: \begin{cases} d(\text{O1}-\text{B}) = 1.374\ \text{Å} \\ d(\text{O2}-\text{B}) = 1.357\ \text{Å} \end{cases}$$

The O1 atom which is farther from its two boron neighbours than O2 is under-bonded whereas the latter is over-bonded. It was observed that the results (MAPD on anion charges) are not really better than those obtained in space group $P3_1$. One might wonder whether $P3_121$ is the highest possible space group for this phase. Analysis by the program *Systre* (Delgado-Friedrichs & O'Keeffe, 2003) of the labelled quotient graph in Fig. 6 shows that embeddings of the periodic net associated with B_2O_3-I with space group $P6_422$ cannot be ruled out. The PSEUDO routine (Capillas *et al.*, 2011) at the Bilbao Crystallographic Server (Aroyo *et al.*, 2006) shows a significant degree of pseudo-symmetry of the structure refined in $P3_121$, which would be compatible with a *translationengleiche* supergroup of the type $P6_422$ with atomic displacements of 0.5013 Å (B), 0.5669 Å (O1) and 0.6968 Å (O2), respectively.

Let us now look at the high-pressure orthorhombic B_2O_3-II phase (Prewitt & Shannon, 1968) with reduced quotient digraph shown in Fig. 7. As in the previous case, charge distribution results for anion-centred polyhedra are trivial; only oxygen values obtained for cation-centred polyhedra are indicated in the figure. Again, weighted average bond lengths provide the same interpretation as for the B_2O_3-I phase. However, a worse MAPD is obtained (0%, 5.5%) clearly evidencing the stress undergone by the high-pressure structure. It is worth noting that pressure-induced coordination changes, from trigonal to tetrahedral for B atoms and from angular to trigonal for one of the two oxygen types, do not completely relax the mechanical stress.

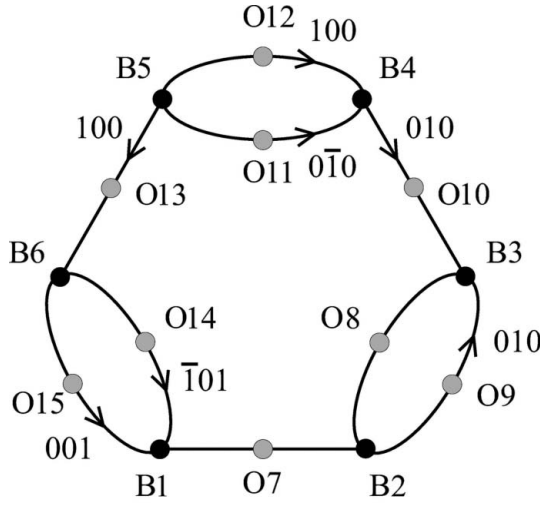

Figure 6
The labelled quotient graph of B_2O_3-I; B atoms are shown in black and O atoms in grey.

4.2. Bi_2O_4

Our second example will illustrate the benefits of the double CHARDI analysis, using both descriptions as cation- and anion-centred polyhedra, combined with the analysis of the bond digraph of the structure to show possible weaknesses in the data. The structure of the mixed-valence (Bi^{3+}, Bi^{5+}) oxide was reported by Kumada *et al.* (1995) who claimed it to be isostructural with β-Sb_2O_4. CHARDI analysis does not give satisfactory results for Bi_2O_4 neither using the description with cation-centred polyhedra (11.4, 17.7%) nor as anion-centred polyhedra (12.8, 19.5%). In comparison, the analysis performed on β-Sb_2O_4 using data from Orosel *et al.* (2005) is a little better: (4.1, 8.6%) with cation-centred polyhedra and (5.1, 10.3%) with anion-centred polyhedra. An interpretation is suggested at the inspection of the reduced bond graphs shown in Fig. 8. Note first that the bond graph of Bi_2O_4 is not consistent; Bi2 makes two bonds with O1 but there is no bond from O1 to Bi2. This is due to a very long Bi2—O1 bond (2.822 Å) with a bond weight of 0.043 which is not even considered from the viewpoint of O1. As a consequence, O2 is over-bonded and O1 under-bonded. The corresponding bond in β-Sb_2O_4 is much shorter (2.356 Å), with a Sb2—O1 bond weight of 0.410 and charges which are better balanced in this structure. The comparison between these structures, which were both obtained by refinement of powder diffraction data, suggests that both may be imprecise, which would not be too surprising considering the large difference in the scattering power of bismuth and oxygen.

It might be argued that inconsistency could be avoided by adding the missing bond to the respective anion- or cation-centred description. However, bond weights and charge

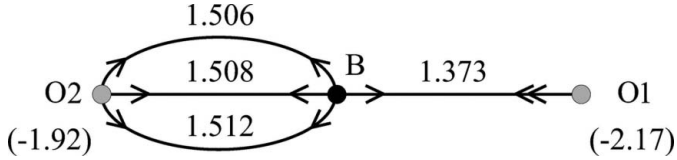

Figure 7
The reduced quotient digraph of the high-pressure B_2O_3-II phase; B atoms are shown in black and O atoms in grey. Bond lengths (Å) are indicated above each edge and charge distribution (CHARDI) computation results for O atoms within brackets.

distributions would not be significantly altered to motivate a new calculation. Besides being arbitrary, the inclusion of the new bond would hide what we think is an intrinsic structural feature. In this sense, inconsistency of the bond digraph points to possible structural problems that are missed in other methods such as BV.

5. Case study

We have extracted a number of well refined recent structures for binary compounds from the Inorganic Crystal Structures Database (ICSD: Belsky *et al.*, 2002) and applied CHARDI analysis. The results are presented in the following different categories:

(i) structures described equally well as cation-centred and anion-centred,

(ii) structures better described as anion-centred but worth-looking as cation-centred, and

(iii) structures advantageously described as anion-centred.

5.1. Structures described equally well as cation-centred and anion-centred

WO_3 crystallizes in several polymorphs, depending on the temperature and pressure. At ambient pressure, the following phases appear on heating: ε (Pc) $\rightarrow$ δ ($P\bar{1}$) $\rightarrow$ γ ($P2_1/n$) $\rightarrow$ β ($Pcnb$) $\rightarrow$ α ($P4/nnc$) (Vogt *et al.*, 1999). A high-pressure polymorph, called HP, has been reported by Xu *et al.* (1997) in $P2_1/c$: this is not a different cell setting of the γ polymorph but the product of a pressure-induced symmetrization of the δ polymorph which is already pseudo-monoclinic. Three neutron powder refinements of the triclinic δ polymorph have been reported by Woodward *et al.* (1995), of which two are from a mixture of δ and γ phases. The quality of the refinement, as judged from the R_{wp} values, was definitely better for the pure triclinic sample (R_{wp} = 0.0789) than for the mixtures of phases (R_{wp} = 0.105 and 0.136). Indeed, the CHARDI analysis for the refinements obtained from the mixture of phases is worse, in both the cation- and the anion-centred description, which points to possible problems in the refinement. For the pure triclinic phase, the results are perfectly satisfactory but do not privilege one description over the other: MAPDs are 0.7% (PC atoms) and 3.8% (V atoms) for the cation-centred description, and 1.4% (PC atoms) and 1.7% (V atoms) for the anion-centred description. For the triclinic structures obtained from a mixture of phases the MAPD values are the following:

R_{wp} = 0.105: 0.020 (PC atoms) and 0.088 (V atoms) in the cation-centred description; 0.029 (PC atoms) and 0.034 (V atoms) in the anion description.

R_{wp} = 0.136: 0.053 (PC atoms) and 0.115 (V atoms) in the cation-centred description; 0.061 (PC atoms) and 0.072 (V atoms) in the anion description.

As shown in §5.3.1, the other polymorphs are better described as anion-centred structures.

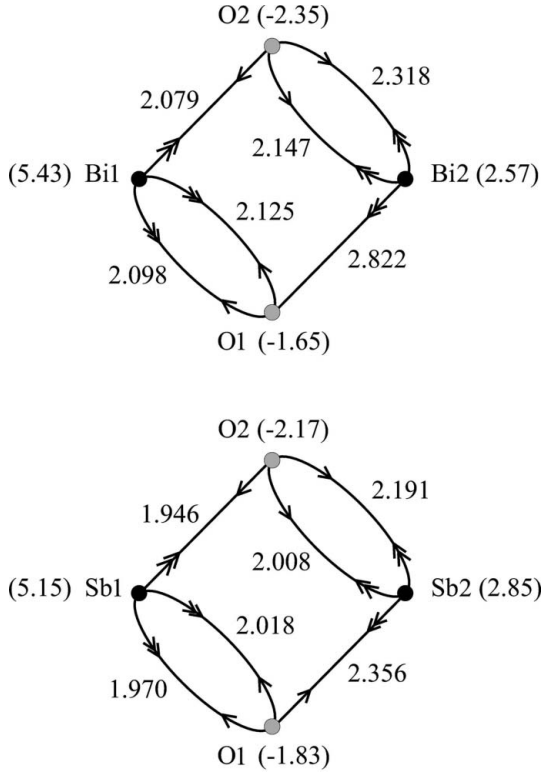

Figure 8
The reduced bond graphs of Bi_2O_4 and β-Sb_2O_4; cations are shown in black and O atoms in grey. Bond lengths (Å) are on the side of the respective edge and charge distribution (CHARDI) computation results for cation-centred polyhedra are given within brackets.

5.2. Structures better described as anion-centred but worth considering as cation-centred: KO_3 as an example

Potassium trioxide (Schnick & Jansen, 1987) is interesting in several aspects. Fig. 9 shows the reduced bond digraph of this structure. At first sight, this digraph does not seem to be very consistent; there is a twofold degenerated edge going from O1 to K2 but no corresponding edge from K2 to O1 (note the

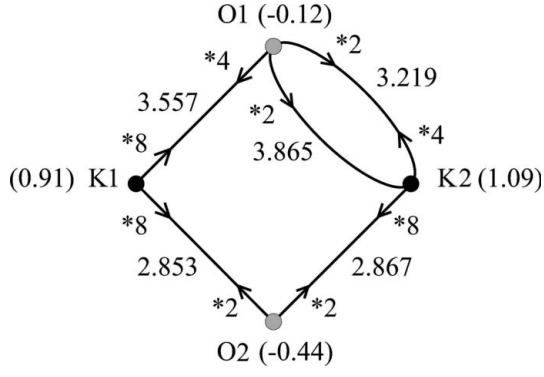

Figure 9
The reduced quotient digraph of KO_3; K atoms are shown in black and O atoms in grey. Bond lengths (Å) are on the side of the respective edge and charge distribution (CHARDI) computation results for cation-centred polyhedra are given within brackets; *n*-fold edge degeneracy is indicated near the corresponding arrow as **n*.

absence of an arrow on this edge on the potassium side). This may be understood by comparing average bond lengths d(O1—K) = 3.446 and d(K2—O) = 2.930 Å. The longer bond with d(K2—O) = 3.865 Å is not considered by CHARDI in the potassium coordination polyhedron.

The anion species in KO_3 is obviously not the oxide ion, but the O_3^- 'ion'. However, CHARDI input charges (formal oxidation numbers) were arbitrarily taken as +1 and −0.33 for potassium and oxygen atom types. With these values, the charge distribution MAPDs were respectively (0.1, 0.4%) and (9, 41.8%) for computation based on anion-centred and cation-centred polyhedra. The good MAPD for anion-centred polyhedra suggests that the structure is well balanced from the viewpoint of O atoms. Hence, charge distributions for cation-centred computation, indicated in the figure, may be considered to obtain new insight into the structure. In this case, charges on O atoms may be interpreted by looking at CHARDI-calculated average bond lengths d(O1—K) = 3.446 Å and d(O2—K) = 2.860 Å. O1 is the central oxygen in the O_3^- species and, being much farther from potassium than terminal O2 atoms (see Fig. 10), charge distributions indicate that it is rather loosely bonded (under-bonded) to potassium. This result is in agreement with the existence of internal O—O bonds in the O_3^- species. Interestingly, however, CHARDI computation results suggest that the central O atom is nevertheless bonded to potassium in this structure.

5.3. Structures advantageously described as anion-centred

5.3.1. WO_3. Of particular interest for our purposes are the monoclinic and triclinic polymorphs, which present more than one crystallographic type of both W and O. The γ polymorph has been studied twice by the same group, from powder neutron diffraction data, with unequal quality of the refinement. The second report (Vogt *et al.*, 1999) was of better quality and shows a markedly better description of the structure as anion-centred (MAPD 0.4 and 0.6% on PC and V atoms, respectively, with respect to 2.2 and 3.5% for a cation-centred description). The cation-centred description presents two highly distorted octahedra (ECoN = 4.73 and 4.25, respectively), whereas the anion-centred description gives six dumbbells, three being close to symmetric (ECoN = 1.99, 1.97 and 1.72 for O1, O2 and O3, respectively) and three highly asymmetric (ECoN = 1.27, 1.09 and 1.10 for O4, O5, and O6, respectively). Interestingly, the most symmetric dumbbells form chains along the ***a*** axis, the least symmetric ones form chains along the ***c*** axes and the intermediate ones form chains along the ***b*** axis.

5.3.2. Magnéli phases. Vanadium oxides V_nO_{2n-1} ($3 \leq n \leq 9$) form a homologous series (Ferraris *et al.*, 2008) known as Magnéli phases (Andersson *et al.*, 1957). The modular structure of these compounds has been described as a sequence of rutile-type (VO_2) slabs separated by crystallographic slip (CS)[4] planes of corundum-type (V_2O_3). Rutile slabs are infinite in two directions and n [VO_6] octahedra wide in the third direction. The structure contains two kinds of parallel chains of octahedra linked by sharing vertices, edges or faces. The rutile block contains linear chains of corner-sharing octahedra; the CS plane contains zigzag chains consisting of double, face-sharing octahedra linked by edge-sharing. It is believed that V^{4+} ions preferentially occupy the zigzag chain. The CS operation occurring at a variable interval in the parent VO_2 structure is a structure mechanism that yields a change in the chemical composition that accompanies the structural change. Such a mechanism is known as *tropochemical cell-twinning* (Takéuchi, 1997; for a more recent review about modular structures see Nespolo *et al.*, 2004). The first terms of the series, namely V_3O_5, V_4O_7 and V_5O_9 display a metal-insulator transition which was interpreted as valence ordering at low temperature.

The high-temperature phase of V_3O_5 = VO_2 + V_2O_3 is monoclinic *I*2/*c* and contains two vanadium crystallographic types. The eightfold V(1) position corresponds to the double octahedra located at the CS plane and the fourfold V(2) position belongs to the rutile slab. Hong & Åsbrink (1982) argued that the ideal valence distribution should be a 50:50 mixture of V^{3+} and V^{4+} on the V(1) type and only V^{3+} on the V(2) type. The low-temperature phase belongs to the *klassengleiche* subgroup *P*2/*c* of index 2 in *I*2/*c*, so that vanadium positions V(1) and V(2) split into V(11), V(12) and V(21), V(22) respectively. At the transition, ordering occurs in the zigzag chains with V^{4+} ideally located at the V(11) position and V^{3+} at the V(12) position.

In fact, using Zachariasen's (1978*b*) equation, Hong & Åsbrink (1982) calculated that the mean valences at positions V(1) and V(2) in the high-temperature phase are 3.42 and 3.15, respectively, not much different from the expected values 3.5 and 3.0. In the same way they showed that the mean valences at positions V(11), V(12), V(21) and V(22) are 3.87, 3.06, 3.06 and 3.07, respectively. These results are consistent with valence ordering in the CS plane.

CHARDI analysis was applied to both structures, using cation-centred and anion-centred polyhedra. As discussed above, the computed charge on the V atoms represents an indication of the formal oxidation number of these atoms, whereas those on the PC atoms are the result of the distribution of input charges. For the cation-centred description, the CHARDI calculation provides an indication of the oxidation number for the anions, which in these examples are established: as expected, the results are in very good agreement

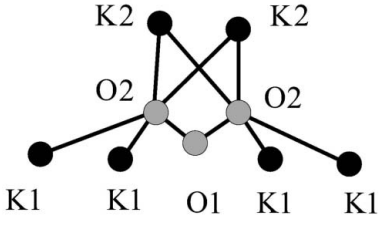

Figure 10
Local structure around O1 in KO_3; O1—K bonds are not shown.

[4] About the use of *crystallographic slip* instead of *crystallographic shear* see Takéuchi (1997)

with the input charges. On the other hand, the oxidation number of the cation sites depends on the distribution of V^{3+} and V^{4+} and the anion-centred description gives a clear indication of this distribution. The computed charges are 3.40 and 3.19 for V(1) and V(2) in the high-temperature phase but 3.90, 3.02, 3.18 and 2.98 for V(11), V(12), V(21) and V(22) in the low-temperature phase, respectively, in good agreement with the results published by Hong & Åsbrink (1982). The results are summarized in Fig. 11, where it is clear from the structure of the bond digraph that they are not trivial. We stress that CHARDI analysis with anion-centred polyhedra does not demand a correct valence for cations in the initial data sheet; instead it is a primary result of the calculation. As these examples clearly show, the method is quite suited to the analysis of mixed-valence oxides.

Both low- and high-temperature $V_4O_7 = V_2O_4 + V_2O_3$ crystallize in the same space-group type ($A\bar{1}$: the unconventional setting is used to keep a common axial reference for the members of the homologous series) with four formula units per unit cell (Marezio *et al.*, 1973). The rutile slabs are four octahedra wide and consist of two non-equivalent finite chains, namely V(3)–V(1)–V(1)–V(3) (chain 3–1) and V(4)–V(2)–V(2)–V(4) (chain 4–2), where V(3) and V(4) belong to the CS plane. Mean valences have been calculated for both structures by Hodeau & Marezio (1978) using Zachariasen's method. They reported for the high-temperature phase (at 298 K) 3.64–3.53 and 3.48–3.35 for chains 3–1 and 4–2, respectively, indicating the statistical distribution of V^{3+} and V^{4+} among the four vanadium positions. The results for the low-temperature phase at 200 K are 3.84–3.83 and 3.11–3.22 for chains 3–1 and 4–2, respectively, suggesting the segregation of V^{4+} on chain 3–1 and V^{3+} on chain 4–2. CHARDI analysis with anion-centred polyhedra provided charges 3.66–3.50 and 3.51–3.34 at 298 K and 3.91–3.80 and 3.17–3.12 at 200 K for chains 3–1 and 4–2, respectively.

As a last example, we look at $V_5O_9 = 3VO_2 + V_2O_3$. The high- and low-temperature phases crystallize in space groups of the type $P\bar{1}$, respectively, in the $B\bar{1}$ and $P\bar{1}$ settings, and display rutile slabs five octahedra wide (Le Page *et al.*, 1991). Twofold vanadium positions have been labelled as V(10) and V(20), while fourfold vanadium positions are labelled as V(11), V(12), V(21) and V(22) in the high-temperature phase. In the low-temperature phase every fourfold position splits into two twofold positions denoted with a prime: V(11) for instance splits into V(11) and V(11′). There are again two kinds of rutile chains in both structures. In the low-temperature phase these are V(12)–V(11)–V(10)–V(11′)–V(12′) and V(22)–V(21)–V(20)–V(21′)–V(22′). The chains in the high-temperature phase are obtained by withdrawing the prime. In the high-temperature structure valences were calculated in the same way as previously by Le Page *et al.* (1991) to be 3.66–3.42–3.55–3.42–3.66 and 3.62–3.56–3.64–3.56–3.62 using the same sequence as above. The mean valence of vanadium in this phase being 3.6; the results indicate a statistical distribution of V^{3+} and V^{4+} among all positions. Accordingly, CHARDI analysis with anion-centred polyhedra provided the charges 3.77–3.46–3.48–3.46–3.77 and 3.68–3.54–3.62–3.54–3.68 following the same sequence. For the low-temperature structure Le Page *et al.* (1991) reported mean valences of 3.80–3.18–3.36–3.23–3.18 and 3.87–3.78–3.86–3.82–3.86 also following the same sequence as above, suggesting that the second chain is fully occupied with V^{4+} while the first chain has a single V^{4+} at one of its ends. CHARDI analysis with anion-centred polyhedra provided similar results: 4.12–3.15–3.21–3.15–3.19 and 4.03–3.80–3.79–3.71–3.85, again following the same sequence as above.

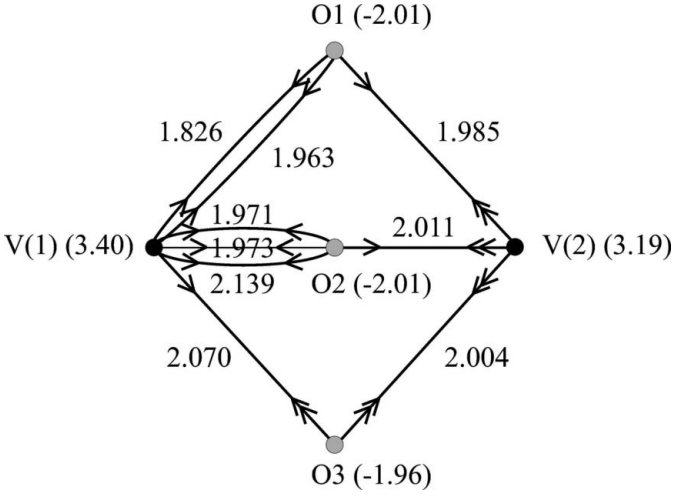

Figure 11
The reduced quotient digraph of the high-temperature V_3O_5; V atoms are shown in black and O atoms in grey. Bond lengths (Å) are on the side of the respective edge and charge distribution (CHARDI) computation results for anion-centred polyhedra are given within brackets

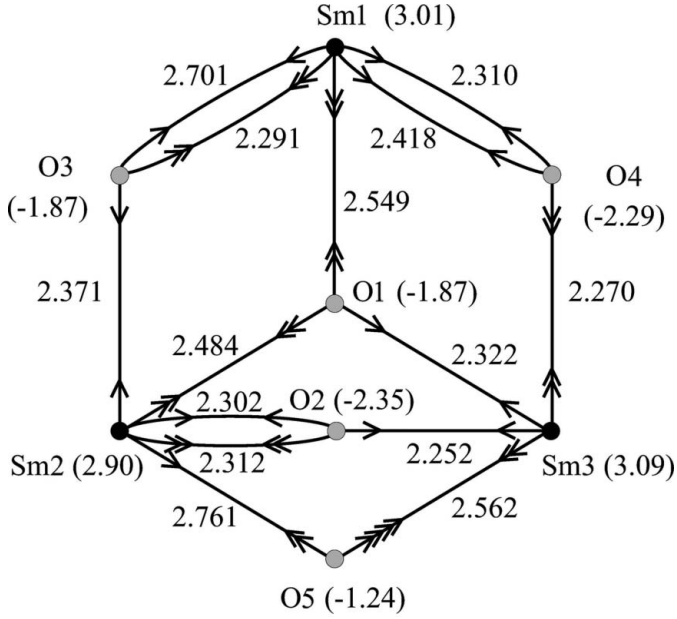

Figure 12
The reduced quotient digraph of monoclinic Sm_2O_3; Sm atoms are shown in black and O atoms in grey. Bond lengths (Å) are indicated on the side of respective edge and charge distribution (CHARDI) computation results for cation-centred polyhedra within brackets.

Table 4
Weighted average bond lengths (Å) and ECoN for monoclinic and cubic Sm_2O_3.

	Monoclinic		Cubic	
	Average distance (Å)	ECoN	Average distance (Å)	ECoN
Sm1—O	2.385	6.13	2.311	6.00
Sm2—O	2.375	6.22	2.356	5.85
Sm3—O	2.324	5.38	–	–
O1—Sm	2.458	4.78	2.343	3.91
O2—Sm	2.293	3.98	–	–
O3—Sm	2.344	3.47	–	–
O4—Sm	2.307	3.91	–	–
O5—Sm	2.607	5.75	–	–

5.3.3. Sm_2O_3. Four isotypic monoclinic sesquioxides, crystallizing in space groups of the type *C*2/*m*, present a charge distribution which is remarkably more satisfactory when described as anion-centred: Er_2O_3 (Wontcheu & Schleid, 2008), Eu_2O_3 (Yakel, 1979), Ho_2O_3 (Hering & Huppertz, 2009) and Sm_2O_3 (Boulesteix *et al.*, 1971; Cromer, 1957). These structures contain three crystallographically independent cation sites (*M*1 to *M*3) and five crystallographically independent anion sites (O1 to O5). They are very closely related, the maximum distance between atomic positions of paired atoms, taking the Er compound as reference, going from 0.028 Å (Ho) to 0.062 Å (second Sm structure), as computed by the *COMPSTRU* routine at the Bilbao Crystallographic Server (Aroyo *et al.*, 2006). The description is given here for the Sm compound; the analyses for the other compounds are closely related, given the tight structural similarity.

Fig. 12 shows the reduced quotient digraph of the monoclinic C-Sm_2O_3 phase (Schleid & Meyer, 1989). This structure is particularly interesting as CHARDI MAPD for the analysis with anion-centred polyhedra is (0.1, 0.1%). In contrast, MAPD for analysis with cation-centred polyhedra is (2.2, 14.6%). Only the charge distributions for the latter computation are displayed in the reduced digraph.

The situation is quite different for the cubic polymorph (Saiki *et al.*, 1985), which yields (0, 5.4%) MAPD for computation with anion-centred polyhedra. The MAPD for cation-centred polyhedra is trivial (0, 0) because of the presence of only one type of anion, as clearly appears in the reduced quotient digraph shown in Fig. 13.

To interpret the significant difference between the monoclinic and cubic phases of Sm_2O_3, we list in Table 4 the weighted average bond lengths and effective coordination numbers (ECoN) in each coordination polyhedron as they are calculated by CHARDI. The first striking piece of information is the average bond length *d*(O5—Sm), much larger than any other. In fact, it is apparent in Fig. 12 that the neighbourhood of O5, with four neighbours at 2.562 Å and two at 2.761 Å, is rather different from that of the other O atoms. This must be compared with the neighbourhoods of the Sm atoms which, in contrast, are much more similar to each other. The three Sm atoms have an ECoN close to 6 with all bond lengths nearly in the same wide range. On the other hand, ECoN for O atoms vary from little more than 3 to almost 6. It is also apparent that the coordination polyhedra of oxygen types display rather well defined geometries. O1 is square-pyramidal with one apical short distance. O2 and O4 coordination polyhedra are irregular tetrahedra. O3 is trigonal pyramidal with an apical long distance. The coordination polyhedron of O5 is an elongated octahedron. In comparison, samarium coordination polyhedra are not well defined. Thus, from the geometrical point of view, the structure appears to be effectively anion-centred.

On the other hand, the cubic polymorph has a much more regular coordination: Sm1 occupies a regular octahedron whereas Sm2 is in a slightly deformed octahedron, the difference resulting from the different type of Wyckoff position occupied by the two atoms. The O atom is instead in a slightly deformed tetrahedron defined by one Sm1 and three Sm2 atoms.

For the isomorphic europium sesquioxide (Yakel, 1979), MAPD computed from anion-centred and cation-centred polyhedra are (0.7, 1.4%) and (2.8, 12.5%), respectively, following precisely the same trend as the samarium compound. Note that Wu *et al.* (2007) have performed *ab-initio* calculations of the structure of the terbium isotype; the results of the CHARDI calculation on these computed structures are (1.5, 2.9%) and (1.5, 13.3%), again confirming the trend seen for the samarium compound.

5.4. Structures with only one type of site

The CHARDI analysis does not apply to structures containing only one type of cation and one type of anion: because there is nothing to distribute, the result is always in perfect accordance.

When a structure contains only a single type of either cation or anion, then the CHARDI analysis applies when this atom is taken as a PC atom [if taken as a V atom then the expression in brackets in the equation for $Q(ij)$ is systematically 1] and the result tells us whether this description is reasonable or not.

Because binary structures tend to be compact and often of rather high symmetry, there are many examples falling in this category.

5.4.1. Li_3N. Both structures of normal-pressure α-Li_3N (Rabenau & Schulz, 1976) and high-pressure β-Li_3N (Beister

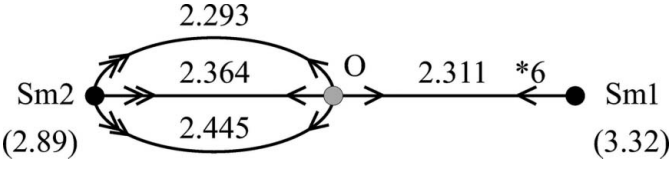

Figure 13
The reduced quotient digraph of cubic Sm_2O_3; Sm atoms are shown in black and O atoms in grey. Bond lengths (Å) are indicated above the respective edge and charge distribution (CHARDI) computation results for cation-centred polyhedra within brackets; the edge out of Sm1 is sixfold (*6) degenerated.

et al., 1988) contain a single type of anion (N^{3-}) and two types of cation (Li^{+}). CHARDI analysis can then be applied using only the anion-centred polyhedra. The results are (0, 3.3%) and (0, 12.4%) for the α and β phases, respectively. The first value (0%) is due to the singleness of the type of anion and conveys no information. The second value indicates a better charge distribution for the α phase. Since the structure of the β phase was refined under ambient conditions, where it is metastable, the unbalanced charge on the cations might indicate that the crystal is under mechanical stress.

6. Discussion

The classical description of non-molecular solids as built on cation-centred polyhedra finds its rationale in the fact that 'anions' (electronegative atoms) have generally larger size than 'cations' (electropositive atoms) because of their higher electronegativity. They thus occupy a significant proportion of the crystal volume, with the cations then being confined in the cavities left empty.

The size of an atom is not such a straightforward concept as it is taught in fundamental chemistry courses. Indeed, the spherical model which is behind the concept of covalent radius is a rough approximation of the real atomic shape in molecular compounds, which is more precisely described by a multipolar model (Hansen & Coppens, 1978). The same also holds true for ionic compounds, as shown by the direction-dependency of the ionic radius in halides, which results in a polyhedral shape for the atomic basins (Pendás *et al.*, 1998). The limits of the concept of ionic radius were long ago recognized by Hoppe (1970), who called it an 'inorganic chameleon' and introduced a 'fictive ionic radius' (FIR) to account for the variation of the polyhedral size of one and the same 'ion' in the same crystal (Hoppe, 1979).

An important consequence of the departure of the atomic shape from the spherical model is that the volume occupied by a cation (anion) is normally larger (smaller) than that assumed by the spherical model. This is in perfect accordance with the fact that the (absolute value of the) real charge of an atom in a crystal, as computed by integrating the electron density in the basin occupied by the atom, is lower than the formal charge attributed to that atom in a classical description within the framework of the valence theory.

A Madelung-type description of a crystal structure like that operated by CHARDI has the advantage of giving a description which is operationally very simple of the topology of the connectivity in the structure, but is by definition limited to a spherical model of the atoms. The results of the more sophisticated approaches cited above show, however, that the relative sizes of the atoms have to be reconsidered. It is thus not surprising that some structures are more satisfactorily described as anion-centred: this is clearly the case for large cations such as Sm_2O_3 and KO_3 discussed here. But even for smaller cations, as in B_2O_3, the alternative anion-centred description can be meaningful.

APPENDIX *A*
Convergence of the mean PC—V distance

For the sake of clarity we rewrite the iteration expressions in equation (1) as

$$f(D) = \frac{\sum_i d(i)w(i)}{\sum_i w(i)}$$
$$w(i) = \exp\left\{1 - \left[\frac{d(i)}{D}\right]^6\right\}, \qquad (9)$$

where:

(i) the sums run over a single index i representing both crystallographic types of V atoms and distances within the first coordination sphere,

(ii) $d(i)$ and $w(i)$ are the respective distances and weights and

(iii) D is a variable.

The new index is required to satisfy $d(i) \leq d(j)$ whenever $i < j$. Comparison with equation (1) shows that if the mean distance at step n is written as ${}^n d = D$ that at step $n+1$ is given by ${}^{n+1}d = f(D)$. The first derivative f' of function f with respect to D can be written as

$$f'(D) = 6\frac{\sum_{i<j}(d(j) - d(i))(d(j)^6 - d(i)^6)w(i)w(j)}{\left(\sum_i w(i)\right)^2 D^7} > 0, \qquad (10)$$

showing that f is strictly increasing. Let N be the coordination number for the respective polyhedron; because $f(D)$ is a weighted average of distances $d(i)$ for $1 \leq i \leq N$ with positive weights we have $d(1) < f(D) < d(N)$. Hence, ${}^0d = d(1) < f(d(1)) = {}^1d < d(N)$ or ${}^0d < {}^1d < d(N)$, on which inequality we may apply f to obtain ${}^1d = f({}^0d) < f({}^1d) = {}^2d < d(N)$, and by iteration over n: ${}^0d < {}^1d < {}^2d < \cdots < {}^n d < {}^{n+1}d < \cdots < d(\mathrm{N})$. The sequence ${}^n d$ is thus strictly increasing and limited, which proves that it is convergent.

APPENDIX *B*
The labelled quotient graph of B_2O_3

It is possible to use the package *TOPOS* to obtain the labelled quotient of any crystal structure; for each edge AB in the quotient graph, the program indicates the translation t such that atom A and the translated $t(B)$ are bonded in a three-dimensional structure, where both A and B belong to the origin unit cell. The result, displayed in Fig. 6, is called a labelled quotient graph (Chung *et al.*, 1984). There, required translations t are indicated as vector labels (voltages) of oriented edges. For example, edge B5—O13 is oriented from B5 to O13 and has vector label 100, which means that the atom of type B5 in the origin unit cell is bonded to the translated atom O13 by 100. Note that labelled quotient graphs are oriented, not directed. A directed edge may only be crossed following its direction. An oriented edge may be crossed in both ways; of course vector labels must be changed accordingly. For example, edge O13–B5 has vector label $\bar{1}00$ and so links atom O13 in the origin unit cell to the translated of atom B5 by $\bar{1}00$.

APPENDIX *C*
Glossary

Bond digraph	The directed graph associated with the asymmetric unit of a crystal structure.
Bond graph	The graph describing the framework of a crystal structure. Also the graph describing the asymmetric unit where this may be defined.
Digraph	In a digraph (directed graph), every edge is a directed edge.
Directed edges	Directed edges are only one-way. A directed edge UV cannot be crossed from V to U.
Graph	A graph is determined by a set of vertices, a set of edges and a mapping associating a pair of vertices to every edge. An edge e mapped to the pair of vertices $\{U,V\}$ is generally written $e = UV$. These pairs are unordered: UV and VU are the same edge.
Oriented edges	In a graph with an orientation, edges may be crossed in any way but edge VU is the opposite of edge UV.
Point lattice	A crystallographic orbit obtained by applying the $P1$ t-subgroup of the space group G.
Quotient graph	The graph of the orbits in the bond graph of a crystal structure for the full translation subgroup of its space group.
Vertex-orbit	The set of all the vertices mapped one to the other by the operations in a symmetry group.
Voltage over an edge	The symmetry operation attributed to an edge in a graph with an orientation. When the edge UV in a symmetry-labelled quotient graph has voltage γ the vertex from vertex-orbit U in the crystal structure indexed by the symmetry operation g (*i.e.* vertex $U[g]$ in U) is linked to the vertex from vertex-orbit V indexed by the symmetry operation $g\gamma$ (*i.e.* $V[g\gamma]$).

J.-G. Eon thanks CNPq, Conselho Nacional de Desenvolvimento e Pesquisa of Brazil, for support during the preparation of this work as well as Université de Lorraine (France) for two stays in the years 2011 and 2014. The critical comments of two anonymous referees are thankfully acknowledged.

References

Andersson, S., Collectén, B., Kuylenstierna, U., Magnéli, A., Magnéli, A., Pestmalis, H. & Åsbrink, S. (1957). *Acta Chem. Scand.* **11**, 1641–1652.

Aroyo, M. I., Perez-Mato, J. M., Capillas, C., Kroumova, E., Ivantchev, S., Madariaga, G., Kirov, A. & Wondratschek, H. (2006). *Z. Kristallogr.* **221**, 15–27.

Bader, R. (1994). *Atoms in Molecules: A Quantum Theory*. Oxford: Clarendon Press.

Beck, H. P. (2014). *Z. Kristallogr.* **229**, 473–488.

Beister, H. J., Haag, S., Kniep, R., Strössner, K. & Syassen, K. (1988). *Angew. Chem. Int. Ed. Engl.* **27**, 1101–1103.

Belsky, A., Hellenbrandt, M., Karen, V. L. & Luksch, P. (2002). *Acta Cryst.* B**58**, 364–369.

Blatov, V. A., Shevchenko, A. P. & Proserpio, D. M. (2014). *Cryst. Growth Des.* **14**, 3576–3586.

Boulesteix, C., Pardo, B., Caro, P. E., Gasgnier, M. & la Blanchetais, C. H. (1971). *Acta Cryst.* B**27**, 216–219.

Brown, I. D. (1978). *Chem. Soc. Rev.* **7**, 359–376.

Capillas, C., Tasci, E. S., de la Flor, G., Orobengoa, D., Perez-Mato, J. M. & Aroyo, M. I. (2011). *Z. Kristallogr.* **226**, 186–196.

Chung, S. J., Hahn, Th. & Klee, W. E. (1984). *Acta Cryst.* A**40**, 42–50.

Cromer, D. T., (1957). *J. Phys. Chem.* **61**, 753–755.

Delgado-Friedrichs, O. & O'Keeffe, M. (2003). *Acta Cryst.* A**59**, 351–360.

Effenberger, H., Lengauer, C. L. & Parthé, E. (2001). *Monatsh. Chem.* **132**, 1515–1517.

Engel, P., Matsumoto, T., Steinmann, G. & Wondratschek, H. (1984). *Z. Kristallogr.* Suppl. Issue No. 1.

Eon, J.-G. (2012). *Struct. Chem.* **23**, 987–996.

Ferraris, G., Makovicky, E. & Merlino, S. (2008). *Crystallography of Modular Materials*. Oxford University Press.

Fischer, D. & Jansen, M. (2002). *Angew. Chem. Int. Ed.* **41**, 1755–1756.

Gurr, G. E., Montgomery, P. W., Knutson, C. D. & Gorres, B. T. (1970). *Acta Cryst.* B**26**, 906–915.

Hansen, N. K. & Coppens, P. (1978). *Acta Cryst.* A**34**, 909–921.

Hering, S. A. & Huppertz, H. (2009). *Z. Naturforsch. B*, **64**, 1032–1040.

Hodeau, J.-L. & Marezio, M. (1978). *J. Solid State Chem.* **23**, 253–263.

Hong, S.-H. & Åsbrink, S. (1982). *Acta Cryst.* B**38**, 713–719.

Hoppe, R. (1970). *Angew. Chem. Int. Ed. Engl.* **9**, 25–34.

Hoppe, R. (1979). *Z. Kristallogr.* **150**, 23–52.

Hoppe, R., Voigt, S., Glaum, H., Kissel, J., Müller, H. P. & Bernet, K. (1989). *J. Less-Common Met.* **156**, 105–122.

Klein, H.-J. (1996). *Math. Model. Sci. Comput.* **6**, 325–330.

Krivovichev, S. V. (2009). *Structural Crystallography of Inorganic Oxysalts.* IUCr Monograph on Crystallography 22. Oxford University Press.

Krivovichev, S. V., Mentré, O., Siidra, O. I., Colmont, M. & Filatov, S. K. (2013). *Chem. Rev.* **113**, 6459–6535.

Kumada, N., Kinomura, N., Woodward, P. M. & Sleight, A. W. (1995). *J. Solid State Chem.* **116**, 281–285.

Le Page, Y., Bordet, P. & Marezio, M. (1991). *J. Solid State Chem.* **92**, 380–385.

Marezio, M., McWhan, D. B., Dernier, P. D. & Remeika, J. P. (1973). *J. Solid State Chem.* **6**, 419–429.

Mills, S. J., Christy, A. G., Chen, E. C. C. & Raudsepp, M. (2009). *Z. Kristallogr.* **224**, 423–431.

Nespolo, M., Ferraris, G., Ďurovič, S. & Takéuchi, Y. (2004). *Z. Kristallogr.* **219**, 773–778.

Nespolo, M., Ferraris, G., Ivaldi, G. & Hoppe, R. (2001). *Acta Cryst.* B**57**, 652–664.

Nespolo, M., Ferraris, G. & Ohashi, H. (1999). *Acta Cryst.* B**55**, 902–916.

Orosel, D., Balog, P., Liu, H., Qian, J. & Jansen, M. (2005). *J. Solid State Chem.* **178**, 2602–2607.

Parthé, E. (1996). *Elements of Inorganic Structural Chemistry*, 169 pp. Petit-Lancy, Switzerland: K. Sutter Parthé Publisher.

Pauling, L. (1929). *J. Am. Chem. Soc.* **51**, 1010–1026.

Pendás, A. M., Costales, A. & Luaña, V. (1998). *J. Phys. Chem. B*, **102**, 6937–6948.

Prewitt, C. T. & Shannon, R. D. (1968). *Acta Cryst.* B**24**, 869–874.

Rabenau, A. & Schulz, H. (1976). *J. Less-Common Met.* **50**, 155–159.

Saiki, A., Ishizawa, N., Mizutani, N. & Kato, M. (1985). *J. Ceram. Soc. Jpn*, **93**, 649–654.

Schleid, T. & Meyer, G. (1989). *J. Less-Common Met.* **149**, 73–80.

Schnick, W. & Jansen, M. (1987). *Rev. Chim. Miner.* **24**, 446–456.

Takéuchi, Y. (1997). *Tropochemical Cell-Twinning. A Structure Building Mechanism in Crystalline Solids*, 319 pp. Tokyo: Terra Scientific Publishing Company.

Vogt, T., Woodward, P. M. & Hunter, B. A. (1999). *J. Solid State Chem.* **144**, 209–215.

Wontcheu, J. & Schleid, T. (2008). *Z. Anorg. Allg. Chem.* **634**, 2091.

Woodward, P. M., Sleight, W. & Vogt, T. (1995). *J. Phys. Chem. Solids*, **56**, 1305–1315.

Wu, B., Zinkevich, M., Aldinger, F., Wen, D. & Chen, L. (2007). *J. Solid State Chem.* **180**, 3280–3287.

Xu, Y., Carlson, S. & Norrestam, R. (1997). *J. Solid State Chem.* **132**, 123–130.

Yakel, H. L. (1979). *Acta Cryst.* B**35**, 564–569.

Zachariasen, W. H. (1931). *Z. Kristallogr.* **80**, 137–153.

Zachariasen, W. H. (1978*a*). *J. Less-Common Met.* **62**, 1–7.

Zachariasen, W. H. (1978*b*). *Acta Cryst.* A**34**, s406.

Zarychta, B., Pichon-Pesme, V., Guillot, B., Lecomte, C. & Jelsch, C. (2007). *Acta Cryst.* A**63**, 108–125.